PAPER

Check for updates

Thermoelectric property enhancement of single-wall carbon nanotube network by ICl intercalation and filling: a first-principles study†

Md. Mafizul Islam [ID] [ab] and Ahmed Zubair [ID] *[a]

CNTs are promising candidates for wearable thermoelectric applications because of their simultaneously prevailing features of flexibility, lightweight, and quantum confinement due to low dimensionality. The unique advantages of CNT's one-dimensionality can be extracted by tuning the Fermi level near the singularity points of the density of states at the band edges by doping the CNT network. Though interhalogen compounds act as excellent dopants among the various dopants in the CNT system, the impact of their orientation and placement in the CNT system is rarely explored. Here, we investigated the impact of ICl molecule filling and intercalation and its orientation on the thermoelectric properties of a semiconducting single-wall carbon nanotube (SWCNT) network through density functional theory (DFT)-based *ab initio* calculations and Boltzmann transport theory. Our calculated ICl-doped SWCNT system showed improved thermoelectric performance. Notably, the system's power factor can be increased from 0.28 to 2.4 mW m^{-1} K^{-2}, more than an eight-fold increment of its value obtained at the Fermi level. On the other hand, ICl intercalation of the SWCNT bundle shifted the peak thermoelectric power factor below its Fermi level, and it can be attained by doping the CNT bundle with additional acceptor atoms. We achieved the best enhancement of the thermoelectric power factor from zero for pristine CNTs to 0.3 mW m^{-1} K^{-2} when the ICl molecules were horizontally aligned outside the CNTs in close spacing with adjacent dopants. It can further be pulled up to 1.82 mW m^{-1} K^{-2} by doping the CNT with an acceptor concentration of 7.1×10^{21} cm^{-3}. The insights gained in this investigation will help design and fabricate substrate-supported and flexible thermoelectric nanogenerators and coolers for applications to power up wearable electronics and IoT-based remote devices where thermal energy is abundant.

1 Introduction

The demand for flexible and portable energy-harvesting devices to power up wearable electronics and IoT-based devices is increasing day by day. A significant amount of energy is being wasted as heat worldwide, and this thermal energy can be converted to electrical energy through a thermoelectric nano-generator (TEG). The TEG is a solid-state electronic device that directly converts thermal energy into electrical energy and *vice versa*.[1–3] Moreover, the TEG can be used as a solid-state cooler for electronic chips. The key performance parameter for converting thermal energy into electrical energy is the power factor,

defined as $S^2\sigma$, where S represents the Seebeck coefficient and σ denotes the material's electrical conductivity. Furthermore, a large power factor is needed for solid-state active cooling, which utilizes the Peltier effect to enhance the heat flow rates from the heat source to the surroundings. However, especially for wearable applications, the TEGs must have some unique features, such as flexibility, washability, and comfort. Commercially available conventional thermoelectric materials such as Bi$_2$Te$_3$, PbTe, and their alloys have good thermoelectric power factor ($\sim$1.5–4.5 mW m^{-1} K^{-2}) at room temperature.[1] However, their toxicity, scarcity, and rigidity limit their use in wearable applications. A record high thermoelectric power factor was reported recently for low-dimensional thermoelectric materials, such as $\sim$37 mW m^{-1} K^{-2} for graphene and 26 mW m^{-1} K^{-2} for ultra-thin FeSe.[4,5] However, these record-high PF values were found in their tiny flakes, and their scalability is yet to be explored. In addition, a physics dilemma is the trade-off relationship between S and σ in the charge neutrality region of semiconducting materials.[6] According to Hicks and Dresselhaus, this

[a] Department of Electrical and Electronic Engineering, Bangladesh University of Engineering and Technology, Dhaka 1205, Bangladesh.
E-mail: ahmedzubair@eee.buet.ac.bd

[b] Department of Textile Machinery Design and Maintenance, Bangladesh University of Textiles, Dhaka 1208, Bangladesh

trade-off relationship between S and σ can be solved by using low-dimensional materials in thermoelectric devices.[7–9] In low-dimensional materials, the movement of charge carriers is limited to certain directions. For example, electrons in one-dimensional (1D) materials can move in a single direction and are confined in the other two directions, which leads to a narrow carrier distribution channel. The shifting of the Fermi level (E_F) at the van Hove singularity (VHS) at the edge of the charge neutrality gap in the density of states (DOS) enhances the electrical conductivity. In addition, the Seebeck coefficient has a decent value in the VHS peaks at the band edge, which enhances the power factor.

Among the low-dimensional materials, carbon nanotubes (CNTs), a 1D material, are expected to possess excellent thermoelectric performance. Additionally, CNTs have promising characteristics such as high electrical conductivity, thermal conductivity, mechanical strength, aspect ratio, and lightweight.[3,10,11] CNTs can be fabricated into highly flexible fibers, which can be knitted into fabrics along with washability and good comfort.[10] The 1D quantum mechanical features for thermoelectric performance are readily attainable in CNTs due to their inherent diameter within the de Broglie wavelength.[1,12] The E_F is required to shift at the VHS of the band edges to achieve improved thermoelectric performance.[13,14] The shifting of E_F can be obtained by doping the CNTs.[15–18] Among several CNT dopants, the well-known chlorosulfonic acid doping on the CNTs enhanced the electrical conductivity of the doped CNT system.[15,19,20] Damien *et al.* reported an approximate Fermi level shift of ~ -0.7 eV, resulting in a p-type CNT system achieved through doping with chlorosulfonic acid[15] and they enhanced the electrical conductance of the doped CNT fiber by approximately a factor of five. The halogens and their compounds are efficient doping agents for high electrical conductivity and improved thermoelectric performance of CNTs.[16,20–22] Iodine is an effective CNT dopant with high electrical conductivity, which forms mono and poly-iodide inside the tubes and makes an iodine chain.[16,23] The iodine molecules remove electrons from the carbon atoms of CNTs, which results in p-type doping. Zubair *et al.* reported a significantly enhanced electrical conductivity (~ 6.5 MS m^{-1}) of iodine-doped CNT fibers, which was better than chlorosulfonic acid-doped CNT networks.[16] For bromine doping, CNTs shared the electrons from carbon with bromine, and the doped CNT network becomes p-type with enhanced electrical conductivity.[24] The interhalogen compounds iodine monochloride (ICl) and iodine monobromide (IBr) are also efficient CNT dopants for improving electrical conductivity. Janas *et al.* improved the electrical conductance of ICl and IBr-doped CNT bundles by $\sim 2–3$ times without causing any unwanted modification of the CNT system.[25,26] In addition, ICl is a stable CNT dopant with increased electrical conductivity.[22,25,26] No electrical conductivity degradation was observed while the ICl-doped CNT fibers underwent repeated bending and showed thermal stability at elevated temperatures in practical thermoelectric devices.[22,25] The fabrication process of ICl doping onto CNT fiber is an easy process through vapor-phase doping. The evaporation of ICl in the presence of wet-spun CNT fibers and annealed (350–500 °C) for a short duration (~ 4 hours) made the process easy and cheap.[22,27] Moreover, the flexibility, knittability, washability, and scalability of ICl-doped CNT fibers were reported with their application of sewing into fabric.[22] Hence, ICl is an effective dopant for carbon nanostructures, and its effect is permanent; unlike iodine, it does not diminish over time.[25] Though there have been reports on CNT doping by different halogen compounds, the impact of the dopant filling inside CNTs and orientation of halogen compounds in dopant intercalated CNTs, such as horizontal and vertical alignment of dopants, have been rarely explored.

In this paper, we comprehensively studied the impact of the orientation of ICl molecules with intercalated (between adjacent SWCNTs) and filled (inside the tube) conditions on the CNT networks using density functional theory (DFT)-based first-principles calculations and Boltzmann transport theory-based transport calculations. We computed the orbital projected band structures ($E - k$), DOS, electrical conductivity, Seebeck coefficient, and thermoelectric power factor at different orientations of the ICl molecules. The ICl molecules were oriented at six different orientations: inside the tube, vertically placed very closely spaced with neighboring dopants (C1) and far from the adjacent dopants (C2); outside the tube horizontally placed with close spacing (C3), far from the adjacent dopants (C4); vertically placed with close spacing (C5); and vertically placed far from the adjacent dopants (C6). We investigated a significant impact on the thermoelectric properties of doping orientation and spacing. Additionally, we studied the temperature dependency on thermoelectric properties of the ICl intercalated and filled SWCNT bundles. Our findings would be beneficial to design CNT-based TEGs for both flexible and substrate-supported electronic and thermoelectronic applications.

2 Computational details

The structural optimization and electronic properties of the doped CNT system were calculated using an *ab initio* and plane wave basis set pseudopotential method in the Quantum ESPRESSO (QE) simulation package.[28] The projector-augmented wave (PAW) pseudopotentials were utilized, and the exchange–correlation functional was described by the Perdew–Burke–Ernzerhof (PBE) parameterization within the generalized gradient approximation (GGA). The Kohn–Sham orbitals were extended with an energy cut-off and charge density cut-off of 50 Ry and 400 Ry, respectively. Using nano-structure builder code, we built a bundle of (8,0) SWCNTs considering a hexagonal honeycomb structure. A super-cell size of ($1 \times 1 \times 5$) was created to accommodate the dopant molecules. The bundle of (8,0) SWCNTs was doped by the ICl compound from different orientations, such as horizontal, vertical, closely spaced, and far from the neighboring dopants, as well as positioning inside and outside the tube. We studied six different orientations of the ICl doped structures and defined the doped structures where the ICl molecules were vertically placed inside the CNT with very close spacing as the C1 configuration, vertically placed inside the CNT with a distance from each other as the C2 configuration, horizontally oriented dopants with

close spacing outside the CNT as the C3 configuration, horizontally placed dopants with a distance from each other as the C4 configuration, vertically placed very closely spaced outside the CNT as the C5 configuration, and vertically placed far from each other outside the CNT as the C6 configuration.

The doped CNT systems were relaxed until they satisfied the force convergence threshold and total energy convergence threshold of 10^{-4} eV Å^{-1} and 10^{-6} eV, respectively. The Broyden–Fletcher–Goldfarb–Shanno (BFGS) algorithm was utilized to relax the structure. The first irreducible Brillouin zone was sampled by Monkhorst–Pack k-grid of $(1 \times 1 \times 5)$ for both geometry optimization and self-consistent field (SCF) calculations. The band structures were calculated in the irreducible first Brillouin zone with a hexagonal k-path (Γ–M–K–Γ–A–L–H–A|L–M|K–H). For non-self-consistent field (NSCF) calculations, a densely sampled $(1 \times 1 \times 50)$ k-grid was used to ensure high accuracy of the computed electronic and thermoelectric properties. We projected the atomic orbitals on the $E - k$ plot of doped SWCNT bundles to better comprehend the electronic property alteration with doping orientations by highlighting the weight of suborbital contributions of the constituent host and guest atoms.

The charge density of the SWCNT bundle and ICl molecules was calculated by performing SCF calculations and later using a post-processing tool to accumulate the charge in a cube file using QE. The difference in charge density between the CNT and ICl compounds was calculated by subtracting the charge density of the dopants from that of the host material. Bader charge analysis was performed on the charge density file as implemented in the program of Henkelman's group to comprehend the sharing of charge among atoms better.[29]

The thermoelectric transport parameters, such as Seebeck coefficient S, electrical conductivity σ, and thermoelectric power factor (PF), were determined using Boltzmann transport theory within constant relaxation time approximation as implemented in the BoltzTraP code.[30] The thermoelectric transport parameters were calculated with three-point interpolation at room temperature, and the interpolated results were integrated within a chemical potential range. A temperature dependence S, σ, and PF were calculated within 200 to 1000 K temperature with a step of 50 K at a certain chemical potential, where the respective parameter was showing its peak.

3 Results and discussion

3.1 Structural properties

The supercell of doped (8,0) SWCNT contained a total of 166 atoms, of which the host material (carbon atoms) and the dopant molecules (ICl) interacted with each other as seen in Fig. 1. Consequently, they formed different compounds and separated atoms of iodine and chlorine depending on their position and orientation, such as inside the tube, outside the tube, perpendicular, and parallel to the tube axis. The optimized pristine (8,0) SWCNT diameter was 6.35 Å, a well-matched geometry with the previous reports.[31,32]

At first, three ICl compounds were placed vertically inside the tube in close spacing (C1). After geometry optimization, the
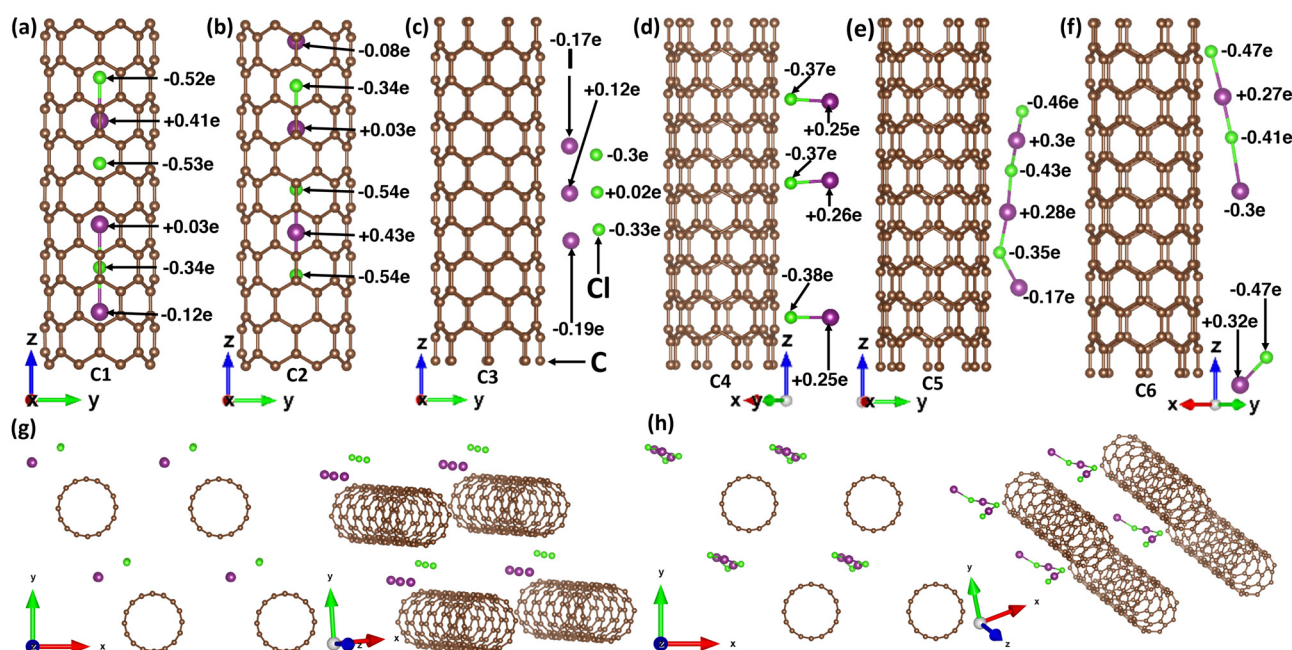

Fig. 1 The side views of the (8,0) SWCNTs doped by three ICl molecules, which were placed: (a) inside and parallel to the tube with very close spacing (C1) to represent high doping concentration; (b) inside and parallel to the tube slightly distant (C2) to represent moderate doping concentration; (c) outside and perpendicular to the tube with very close spacing (C3); (d) outside and perpendicular to the tube slightly distant (C4); (e) outside and parallel to tube with very close spacing (C5); (f) outside and parallel to the tube slightly distant from neighboring dopants (C6). Different planar representations of the bundle form of the ICl-doped SWCNT system. (g) ICl molecules are in close spacing in horizontal orientation outside the CNT (C3), and (h) vertically placed ICl molecules outside the SWCNT in close spacing (C5).

interaction of the dopant with the host material resulted in an I_2Cl and one ICl_2 compound, as can be seen in Fig. 1(a). The bond length between an iodine and a chlorine atom in I_2Cl and ICl_2 compounds was within 2.5 to 2.6 Å. They shared charges with the atoms of the host material and neighboring dopants, which was validated by Bader partitioning of the charge density of the doped CNT system. The charge sharing was also evident from the charge density difference (CDD) plot, as depicted in Fig. 2(a). The yellow color represented charge accumulation, while the cyan color indicated charge depletion. Due to their high electronegativity, the chlorine atoms received more charges than the iodine atoms. We placed them inside the tube vertically and slightly far from each other (C2) to observe how ICl compounds interact with neighboring ICl molecules and host materials. As with the previous structure, this CNT system resulted in an ICl_2 and an I_2Cl compound, as depicted in Fig. 1(b). Their bond distance between two atoms was within 2.5 Å to 2.6 Å. In both CNT systems, the I_2Cl molecule received charges from nearby carbon atoms. One of the iodine atoms transferred a $0.03e$ charge and made it positively charged, and another one received charges from the nearby carbon atoms, resulting in a negatively charged iodine. On the contrary, a greater amount of charge was shared between the atoms of the ICl_2 compound, which indicated strong covalent bonds in ICl_2 (see Fig. 1(a) and (b)). Their CDD plot also validated the formation of ICl_2 and I_2Cl, as seen in Fig. 2(b).

Outside the CNT, we considered four different orientations of three ICl molecules (C3–6). In Fig. 1(c), three ICl molecules were placed horizontally (perpendicular to the tube axis) with very close spacing outside the CNT (C3). A 5 Å vacuum was created perpendicular to the Z-axis to accommodate the dopants. The iodine and chlorine atoms of the top and bottom ICl molecules received charges from the nearby carbon atoms of the host material. A very small amount of charge was transferred from the middle-positioned ICl compound. The small amount of charge sharing indicated weak covalent bonds between the dopant atoms. Consequently, they behaved like separate atoms. The CDD plot also validated this phenomenon, where a depletion of charge occurred between iodine, chlorine, and carbon atoms (see Fig. 2(c)). In contrast, when the ICl

molecules were far from each other (C4) and shared a substantial amount of charge, the chlorine atoms received $\sim 0.37e$, and the iodine atoms transferred $\sim 0.25e$. The significant amount of charge sharing resulted in strong covalent bonds between the iodine and chlorine atoms, and it was also validated by the CDD plot (see Fig. 1(d) and 2(d)). Their bond length was 2.41 Å. When the ICl compounds were placed vertically with very close spacing (C5), they formed a chain of ICl molecules, which is evident from their charge sharing and charge accumulation (see Fig. 1(e) and 2(e)). Their bond distance varied between 2.46 Å and 2.81 Å. In the last structure, the ICl molecules were kept vertically at a distance from each other (C6). The dopants received charges from the carbon atoms, which resulted in the formation of a chain of ICl, as can be observed in Fig. 1(f) and 2(f). The CNTs remained undeformed for all the structures. We showed the initial and optimized structures of the ICl-doped SWCNT network in Section S1 and Fig. S1 of the ESI.†

3.2 Electronic properties

The impact of ICl orientation on the electronic properties of CNTs was analyzed using band structure and density of states (DOS) calculations. The band gap obtained for the pristine (8,0) SWCNT bundle was 0.59 eV, as can be seen in Fig. 3(a). We calculated a full k-path band structure for a pristine (8,0) SWCNT and provided it in Section S2 and Fig. S2 of the ESI.† This band gap agreed with the previous reports for isolated (8,0) SWCNTs.[31,32] It is expected that the GGA-PBE band structure underestimated the band gap. However, a significant contribution near the conduction band minima (CBM) came from the p orbital (88.9%) of the carbon atoms, where the p_z, p_x, and p_y sub-orbital contributions were 2%, 43.5%, and 43.4%, respectively. A few contributions to the CBM came from the s orbital (8.5%). However, in the valence band maxima (VBM), significantly high contribution came from the p_x (50%) and p_y (49.8%) sub-orbitals, where the s and p_z contributed negligibly. The projected density of states (PDOS) validated the band gap obtained in the band structures. As for the band structure, the significant contribution to the total DOS came from the p orbital in a pristine state.
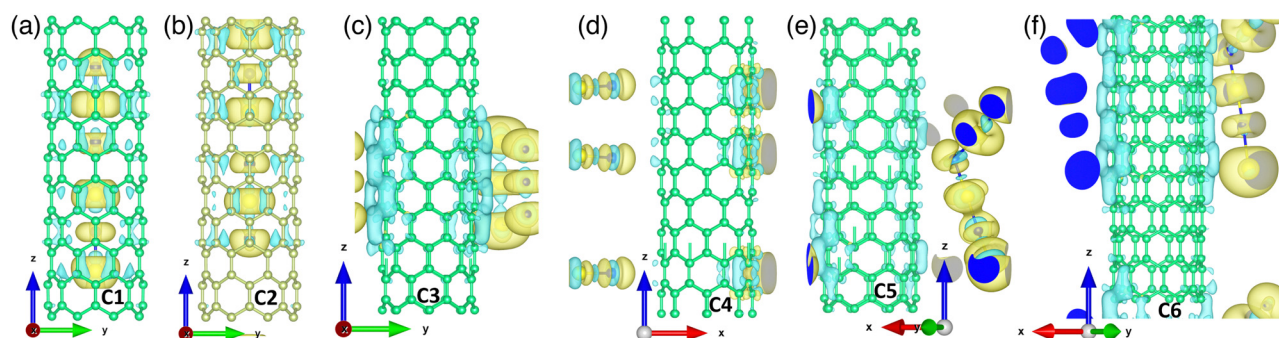

Fig. 2 The charge density difference of the (8,0) SWCNT bundle doped by ICl molecules at different orientations. The ICl molecules are placed (a) inside the tube closely spaced in the vertical orientation (C1), (b) inside the tube and far from each other in the vertical orientation (C2), (c) outside the tube with very close spacing in horizontal orientation (C3), (d) outside the tube in the horizontal orientation and far from each other (C4), (e) outside the tube in the vertical orientation with very close spacing (C5), and (f) outside the tube in vertical orientation and far from each other (C6).
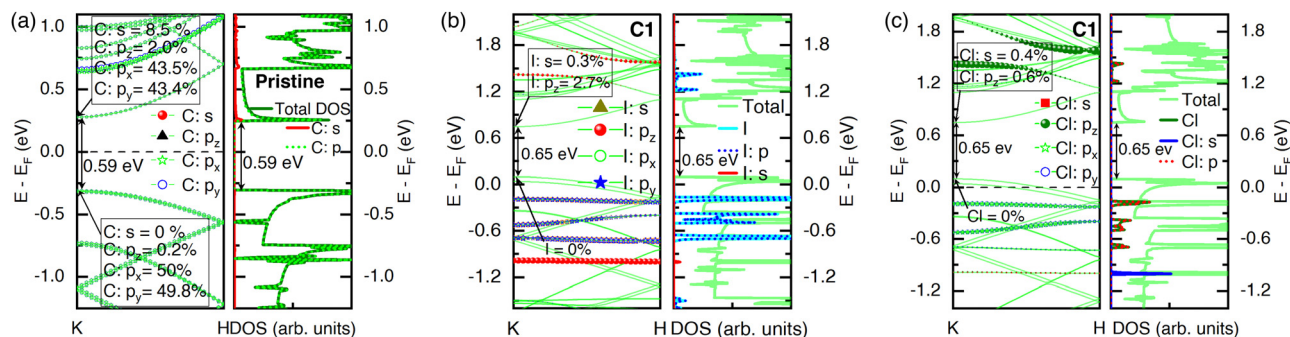
Fig. 3 The orbital projected band structure and density of states (DOS) of (a) a pristine (8,0) SWCNT bundle. Each sub-orbital contribution on the band structure and DOS for (b) iodine and (c) chlorine atoms of ICl molecules when they were doped in a vertical orientation inside the tube with very close spacing (C1).

For a better understanding of the origin of the impact of ICl doping on their electronic structures, we presented the projection of orbitals and sub-orbitals on the band structure of iodine and chlorine atoms in Fig. 3(b) and (c). The orbital projection of iodine and chlorine with suborbital contributions is shown for a particular case when the ICl molecules were placed vertically inside the CNT with very close spacing (C1). In CBM, a small contribution of iodine came from its p_z sub-orbital (2.7%) and s orbital (0.3%), while it did not contribute to the VBM. Iodine atoms contributed substantially to the bands far from the CBM and VBM. The bands formed by iodine above the CBM were contributed by the p_z sub-orbital only. In contrast, all the sub-orbitals of p contributed substantially below the VBM, and its PDOS plot validated that (see Fig. 3(b)). Similar to iodine, the p_z sub-orbital of the chlorine atoms contributed significantly to the bands above the CBM, while it did not take part in the formation of bands below the VBM, as can be observed in Fig. 3(c). In contrast, the bands due to chlorine were mostly contributed by its p_x and p_y sub-orbitals.

The addition of ICl molecules inside the tube (C1 and C2) impacted the bundle of the CNT system as p-type, as evident from the Bader partitioning of charges (see Table 1). The nearby carbon atoms supplied some charges to ICl molecules due to their high electronegativity. It made the whole system p-type and impacted the band structure, making the Fermi level shift below the VBM. The iodine and chlorine atoms contributed a very large amount to the CBM, while no contribution from them was observed in the VBM. The p-type nature was also validated by its PDOS plot, where the significant number of

states of iodine and chlorine were in the valence bands (VB) than that at the conduction bands (CB) (see Fig. 4(a)). When the ICl molecules were placed maintaining a few distances from each other in vertical alignment (C2), there was a small difference—fewer electronic states in the CB. The band gap increased by 0.01 eV, as shown in Fig. 4(b).

The ICl molecules were placed outside the tube in horizontal alignment and closely spaced (C3). In this structure, the iodine and chlorine atoms separated and received charges from the nearby carbon atoms and shared them within themselves. The charge transfer from host to dopant made the CNT system a p-type semiconductor with a band gap of 0.55 eV. Apart from doping inside the tube (C1 and C2), here (C3) the VBM was mainly formed by iodine and chlorine atoms, and the Fermi level shifted by 0.28 eV below its intrinsic position and resided at the edge of the VBM. The carbon, iodine, and chlorine atoms contributed to the VBM by 0.8%, 64.4%, and 34.8%, respectively. On the other hand, iodine and chlorine did not contribute to the CBM, as depicted in Fig. 4(c). However, when the ICl molecules were kept far from each other outside the CNT in horizontal alignment (C4), their band gap decreased by 0.11 eV from its pristine structure, and the contribution to the CBM and VBM was greatly from host atoms, which was associated with a very small amount of charge sharing between the host and dopant molecules. The Fermi level remained in the middle of the band gap due to negligible charge transfer between host and dopant molecules. Rather, iodine and chlorine atoms shared charges within themselves. However, the contribution of ICl molecules to the CBM was 8% and 1.1% in the VBM (see Fig. 4(d)).

The orientation of ICl molecules was changed from horizontal to vertical outside the CNT with very close spacing in configuration C5. A significant amount of charge transfer occurred from host to dopant molecules (see Fig. 1(e)) and, consequently, resulted in the system being p-type with a band gap of 0.55 eV. This phenomenon shifted the Fermi level 0.28 eV below its intrinsic position and it resided on the valence band edge. Furthermore, the VBM was formed by the contributions of iodine and chlorine, while the CBM was mainly established by carbon atoms, as shown in Fig. 4(e). However, when the ICl molecules were placed far from each other (C6),

Table 1 Bader charge analysis of CNT and ICl molecules at different doping orientations

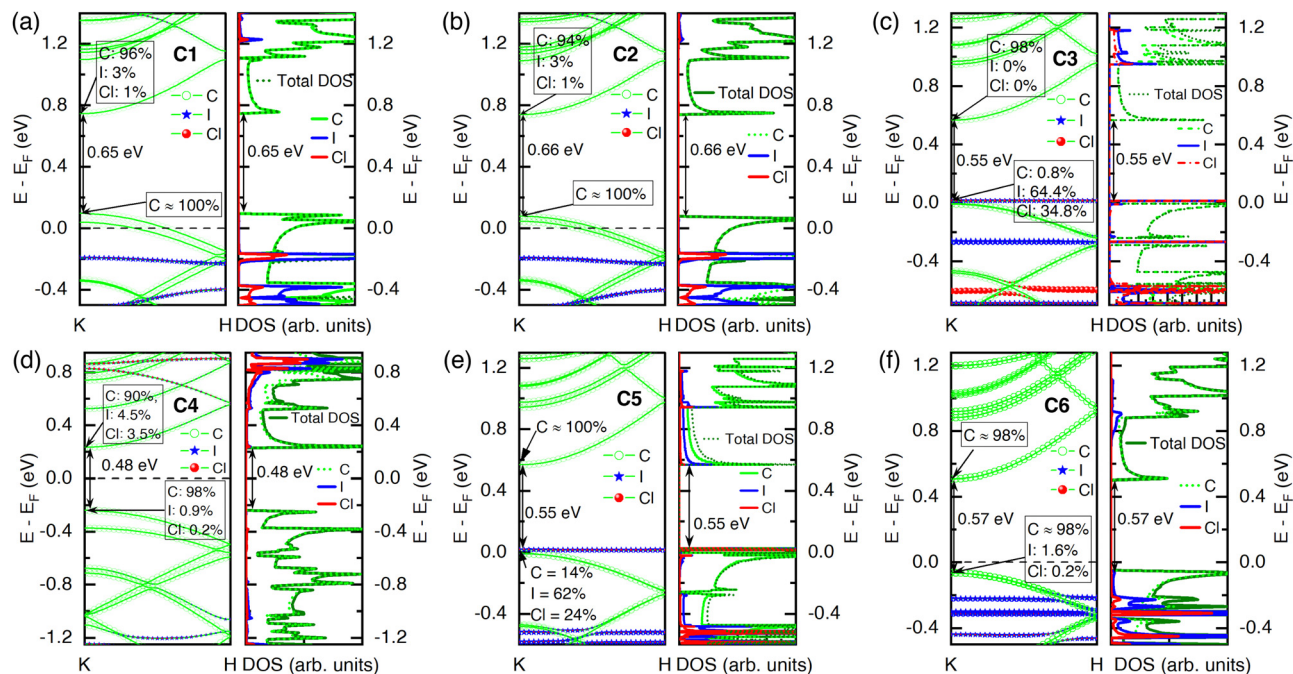| Doping configuration	Bader charge (e)			
	Iodine (I)	Chlorine (Cl)	ICl	CNT (C)
C1	+0.32	−1.39	−1.07	+1.07
C2	+0.38	−1.44	−1.06	+1.06
C3	−0.24	−0.61	−0.85	+0.85
C4	+0.75	−1.11	−0.36	+0.36
C5	+0.40	−1.23	−0.83	+0.83
C6	+0.28	−1.34	−1.06	+1.06

Fig. 4 The orbital projected band structures and DOS of the (8,0) SWCNT bundle doped by ICl molecules at different orientations. The ICl molecules are placed (a) inside the tube and closely spaced in the vertical orientation (C1), (b) inside the tube and far from each other in the vertical orientation (C2), (c) outside the tube with very close spacing in the horizontal orientation (C3), (d) outside the tube in the horizontal orientation and far from each other (C4), (e) outside the tube in the vertical orientation with very close spacing (C5), and (f) outside the tube in the vertical orientation and far from each other (C6).

the amount of charge transfer reduced slightly; nonetheless, the system behaved as p-type. The Fermi level went 0.22 eV below the mid position of the band gap but 0.06 eV above the VBM, as seen in Fig. 4(f). Host atoms contributed significantly to both the VBM and CBM.

In a nutshell, the addition of ICl molecules to the SWCNT, particularly in the C1, C2, and C5 doping orientations, created a substantial amount of electronic energy states inside the charge neutrality region (CNR). Since the iodine and chlorine atoms have higher electronegativity than carbon, they brought out charges from the SWCNT and contributed to the density of states in the doped SWCNT system. A relative shift of the Fermi level below its intrinsic position due to doping by electronegative materials such as ICl made the system p-type.

3.3 Thermoelectric properties

When two junctions of dissimilar metals or semiconductors are placed at different temperatures, a voltage difference (ΔV) occurs between these two junctions. According to the Fermi–Dirac distribution of charge carriers, the electron distribution above the Fermi level increases in the hot region, while it is less in the cold side of the junctions. This is because the charge carriers gain kinetic energy from the heat source and become more agile. Consequently, the electrons above the Fermi level and holes below the Fermi level diffuse from the hot to the cold junction. A difference in Fermi level occurs between two junctions due to uneven carrier distribution, which creates a potential gradient between hot and cold junctions. This phenomenon is known as the Seebeck effect. The potential difference generated per unit

temperature change is quantified as the Seebeck coefficient $S = -\Delta V/\Delta T$. Thermoelectric devices are made of either p-type or n-type materials to obtain a net flow of carriers. Otherwise, the recombination of opposite carriers will lead to no net current. Here, in this study, we doped (8,0) SWCNT bundles by ICl molecules, a p-type dopant for CNTs, to investigate the impact of doping orientation on the thermoelectric properties. We performed first-principles calculations and simulation of the semi-classical Boltzmann transport equation to obtain the thermoelectric transport parameters described by eqn (1) and (2). The Seebeck coefficient S and electrical conductance G were calculated as a function of chemical potential μ.

$$S(\mu) = \frac{1}{qT} \frac{\int dE T_f(E) \left(-\frac{\partial f(E,\mu)}{\partial E} \right)(E - \mu)}{\int dE T_f(E) \left(-\frac{\partial f(E,\mu)}{\partial E} \right)}, \quad (1)$$

$$G(\mu) = \frac{2q^2}{h} \int dE T_f(E) \left(-\frac{\partial f(E,\mu)}{\partial E} \right), \quad (2)$$

Here, q represents the charge of carriers, T is system temperature, and the chemical potential μ depends on the doping level of the CNT system. The transmission function denoted as $T_f(E)$ signifies the likelihood of carrier transport through the materials at a specific energy level E. The Fermi–Dirac distribution function $f(E,\mu)$ characterizes the statistical distribution of electrons with a probability of occupying an energy state at a given temperature.
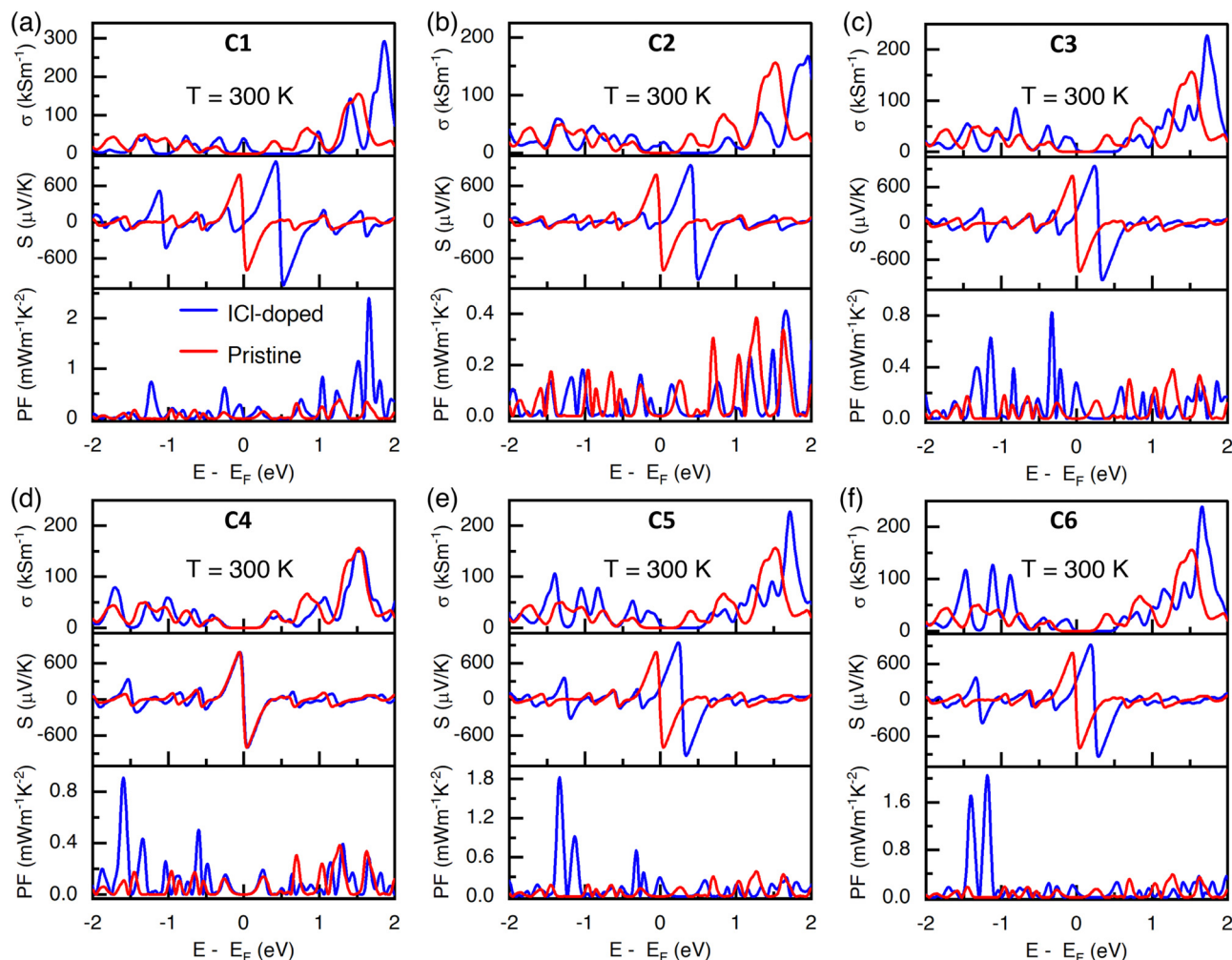
Fig. 5 The electrical conductivity σ, Seebeck coefficient S, and thermoelectric power factor PF as a function of chemical potential μ for the (8,0) SWCNT bundle doped by ICl molecules in different orientations are plotted. The ICl molecules are placed (a) inside the tube closely spaced in the vertical orientation (C1), (b) inside the tube and far from each other in the vertical orientation (C2), (c) outside the tube with very close spacing in the horizontal orientation (C3), (d) outside the tube in the horizontal orientation and far from each other (C4), (e) outside the tube in the vertical orientation with very close spacing (C5), and (f) outside the tube in the vertical orientation and far from each other (C6). The Fermi level is shifted to 0 eV. The red-colored plots are for the pristine (8,0) SWCNT bundle. The results are calculated at T = 300 K.

The change in electrical and thermoelectric transport parameters due to doping is presented in Fig. 5. The electrical conductivity was calculated in terms of carrier relaxation time constant τ. To analyze the impact of dopant orientation on the thermoelectric properties of the ICl-doped (8,0) SWCNT bundle, we took a reference value of τ as 1×10^{-14} s.[33] The electrical conductivity increased by 40 kS m^{-1} when the (8,0) SWCNT bundle was doped by ICl molecules inside the tube vertical to each other in close spacing (C1), as shown in Fig. 5(a). The electrical conductivity increased from zero for pristine to 40 kS m^{-1} and can further be pulled up to 292 kS m^{-1} through doping equivalent to 1.85 eV chemical potential. The Seebeck coefficient increased by 216 μV K^{-1} at 0.42 eV. The maximum power factor was 0.28 mW m^{-1} K^{-2} at the Fermi level. It can further be increased to 2.4 mW m^{-1} K^{-2} by doping the CNT at the chemical potential of 1.65 eV, which is an 8.6-fold increment. The carrier concentration increased due to newly

generated impurity bands, which raised the number of quantum channels for charge transport and increased the number of electronic states at the Fermi level. Consequently, improved σ was obtained for the ICl-doped SWCNT network since it is directly proportional to carrier concentration. An increment of σ and a decent value of S at the Fermi level of the doped system enhanced the thermoelectric power factor ($S^2\sigma$). However, when the ICl molecules were in the same orientation while maintaining a distance from each of them (C2), the σ, and the peak value of S dropped from the state while the dopants were in close spacing (C1) to 167 kS m^{-1} and 946 μV K^{-1}, respectively. The PF was zero at the Fermi level. However, it has chance to slightly increase to 0.41 mW m^{-1} K^{-2} by additionally doping the CNT at the chemical potential of 1.65 eV.

To understand the effect of the horizontal orientation of the ICl molecules, we first placed the dopants outside the tube with very close spacing (C3). As the ICl molecules interacted among

themselves and with the carbon atoms of the CNT, the net charge transfer made the system p-type, which was observed from the band structure where the VBM was formed by a significant contribution of iodine and chlorine atoms and the Fermi level resided at the edge of the valence band. The σ and S increased by 71 kS m^{-1} and 177 μV K^{-1}, respectively (see Fig. 5(c)). The thermoelectric power factor was zero for the pristine (8,0) SWCNT bundle because it had no electronic state at the Fermi level, and consequently, zero electrical conductivity. However, the PF improved by 0.28 mW m^{-1} K^{-2} after doping the CNT for the C3 configuration, and it can further be pulled up to 0.83 mW m^{-1} K^{-2} by doping the CNT with an acceptor concentration of 1.5×10^{21} cm^{-3}. This enhancement of PF for the C3 configuration can be obtained at -0.33 eV chemical potential where a simultaneous peak of both S and σ occurred. The ICl molecules were kept horizontally outside the tube at a slight distance from each other (C4) to observe their impact on the TE performance. In this orientation, a substantial charge transfer happened within the dopant atoms, and a small amount of charge was transferred from the host material to the chlorine atoms. The electrical conductivity and Seebeck coefficient were approximately unaltered due to a negligible amount of charge transfer between the host material and dopant molecules (see Fig. 1(d)). It was also reflected in the band structure, where the VBM and CBM were negligibly contributed by iodine and chlorine atoms (see Fig. 4(d)). The PF was zero at the Fermi level. However, the additional doping of CNTs equivalent to -1.6 eV chemical potential would lift the PF to 0.9 mW m^{-1} K^{-2}.

The vertical alignment of ICl molecules outside the CNT with close spacing (C5) enhanced the TE performance. The system became p-type with a substantial contribution of dopants at the VBM, and the Fermi level resided on the edge of the valence band, as shown in Fig. 4(e). The system became p-type because a significant number of electrons transferred from the host to the dopants, resulting in more electronegative chlorine atoms. The σ and S increased by 71 kS m^{-1} and 157 μV K^{-1}, respectively. The PF enhanced from zero for a pristine CNT to 0.3 mW m^{-1} K^{-2}, and can further be pulled up to 1.82 mW m^{-1} K^{-2} by additionally doping the CNT at -1.33 eV chemical potential (see Fig. 5(e)). In addition, the TE performance was uplifted when the ICl molecules were placed in the same orientation with spacing between their neighbors (C6), as can be seen in Fig. 5(f). In this configuration, σ and S increased by 83 kS m^{-1} and 132 μV K^{-1}, respectively. The peaks of σ increased in the valence band, which was validated by its band structure and DOS, and the iodine and chlorine contributed in the valence band region (see Fig. 4(f)). The partitioning of Bader charge also validated the p-type behavior of the system, where the dopant molecules received a substantial amount of charge from the carbon atoms of the host material (see Fig. 1(f)). For this configuration, the PF enhanced from zero for pristine to 0.13 mW m^{-1} K^{-2}. In addition, a significant increment of PF ~ 2 mW m^{-1} K^{-2} is expected to be attained through further doping the CNT equivalent to -1.2 eV, as can be seen in Fig. 5(f).

For all doping configurations (filling and intercalation) of ICl molecules, the E_F shifted below its intrinsic position, which ensured that the systems were p-type (see Fig. 4). However, the amount of E_F shifting was more pronounced when the ICl molecules were filled inside (C1 and C2) the tube than their intercalation (C3–C6) between adjacent CNTs. It was evident from their band structure and Bader charge analysis, as depicted in Fig. 4 and Table 1, respectively. Owing to the difference in shifting of E_F, the concurrent occurrence of both S and σ were at different chemical potentials for different doping orientations, which impacted their thermoelectric power factor PF ($S^2\sigma$). The peak of S was built when the depletion of charge in DOS occurred; consequently, a lower or close to zero value of σ resulted due to the lack of electronic states there, which maintained an interplay between S and σ. For ICl filled configurations (C1 and C2), the peak of σ resided above and far from E_F with an oscillation. Due to having a high DOS, contributed primarily from C: the p orbital within ~ 1.5–2.0 eV, enhanced the carrier concentration as well as the electrical conductivity for all doping configurations. The fluctuation of DOS created a sharp slope, resulting in a peak of S there. Consequently, a peak of PF was observed above E_F owing to the simultaneous occurrence of a decent value of both σ and S. In contrast, for ICl intercalated CNTs (C3–C6), the concurrent ample values of both S and σ took place below their Fermi level differently from the ICl-filled CNT due to a smaller shift of E_F.

We presented the amount of charge being received ($-$ve) and donated ($+$ve) by each atom of dopant molecules in Table 1. Since the host material consists of only carbon atoms, we did not show the amount of charge transfer for individual carbon atoms. The Bader charge transfer for host (all carbon atoms) and dopant molecules is tabulated in Table 1. A large amount of charge sharing ($\sim 1.06e$) occurred from CNT to ICl molecules for the C1, C2, and C6 doping orientations, as depicted in Fig. 1(a), (b) and (f); and Table 1. This phenomenon produced an increased number of holes in the CNT, which impacted the band structure such that a number of impurity bands were created, especially inside the valence band, and the Fermi level shifted down from its intrinsic position, even E_F shifted inside the valence band for the C1 and C2 orientation, which resulted in a heavily doped p-type system (see Fig. 4(a), (b), and (f)). Secondly, the C3 and C5 orientations shared a high amount of charge ($\sim 0.85e$) from CNT to ICl, which resulted in a downward shifting of E_F and resided at the edge of the valence band in their band structures (Fig. 4(c) and (e)). The shifting of E_F at the band edge near VHS in DOS originated an electrical conductivity, which solved the dilemma of the trade-off relationship between S and σ for the semiconducting CNT. Hence, the thermoelectric power factor (PF) enhanced a reasonable amount, as seen in Fig. 5(a), (c), (e) and (f). Particularly for the C2 configuration, though σ increased, the zero value of S at the E_F resulted in a zero PF for this orientation. Lastly, the least charge transfer occurred for the C4 configuration due to the very far spacing of ICl molecules between their neighbors. This impacted its band structure accordingly with no shifting of E_F and, in turn, did not impact on σ and PF.
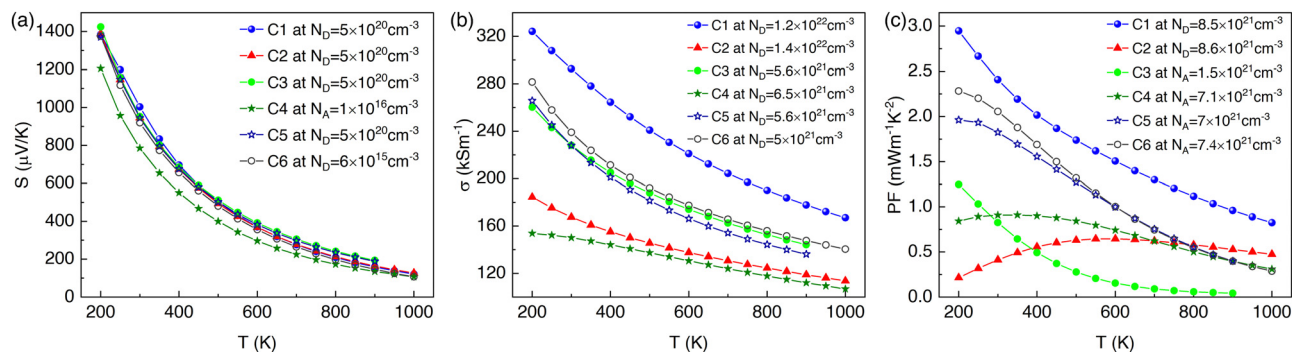
Fig. 6 The impact of change in temperature on the peak values of (a) Seebeck coefficient, (b) electrical conductivity, and (c) thermoelectric power factor for different doping configurations of the SWCNT network.

3.4 Temperature dependency

The impact of a change in temperature on thermoelectric transport parameters is presented in Fig. 6. Here, we show the change of thermoelectric transport parameters at a particular carrier concentration, where they were showing peak performance. A high value of the Seebeck coefficient was obtained at low temperatures. However, it started to decrease with the increase in temperature, mainly due to bipolar transport. The bipolar transport rises with the temperature increase, especially at low carrier concentrations, because minority carrier generation occurs due to thermal excitation. These two effects collectively decreased the value of S with an increase in temperature. The configuration C1 showed the highest value of S near room temperature (see Fig. 6(a)). However, bipolar transport due to carrier generation at elevated temperatures is supposed to increase in such a way that the value of S would decrease more and is expected to cause a sign reversal of S.[34] We calculated the Seebeck coefficient beyond 1000 K, particularly for the C1 doping configuration. Indeed, the effect of bipolar transport was more noticeable and resulted in a considerable decrease of S with even sign reversal beyond 1650 K, as observed in Fig. S3 of the ESI.†

The electrical conductivity σ also showed peak performance for configuration C1 at all temperatures, as shown in Fig. 6(b). The σ started to fall with the elevation of the temperature because the increase in carrier scattering at increased temperatures reduced the electron mean free path, which resulted in a decrease of σ. The peak performance of σ (~ 292 kS m^{-1}) at 1.85 eV chemical potential and room temperature was obtained when the ICl molecules were very closely spaced in vertical alignment inside the CNT (C1).

According to the formula $S^2\sigma$, the combined effect of S and σ represents the thermoelectric power factor, as depicted in Fig. 6(c). The value of PF (~ 0.3 mW m^{-1} K^{-2}) was also highest for the C1, C3, and C5 configurations, where the ICl molecules were in close spacing between their neighbors. However, among the studied doping configurations, the peak value of PF 2.4 mW m^{-1} K^{-2} can be attained by further doping the CNT at a donor concentration of 8.5×10^{21} cm^{-3} for the C1 configuration. The PF increased at low temperatures since both S and σ were the highest at low temperatures. The band gap and peak thermoelectric performance of the ICl-doped (8,0) SWCNT bundle are tabulated in Table 2. Additionally, we achieved a further enhancement of the thermoelectric power factor of ~ 16.6 μW m^{-1} K^{-2} with an ICl concentration of 11.1%. We added an analysis of the dopant concentration-dependent thermoelectric transport parameters in Section S4 and Fig. S4 of the ESI.†

Our study would be beneficial, especially for substrate-free flexible and wearable doped CNT fiber-based thermoelectric nanogenerators, to power up different biosensors as well as IoT-based electronic devices. Additionally, it is also expected to enhance the thermoelectric performance of substrate-supported doped-CNT films such as polymer or oxide-supported doped-CNT films because CNT-polymer junctions lower the thermal conductivity while minimally reducing electrical conductivity, consequently boosting thermoelectric performance.

4 Conclusions

The doping of ICl molecules onto the SWCNT network made the system p-type since electrons transferred from the CNTs to the ICl molecules due to the higher electronegativity of both iodine and chlorine atoms than carbon. The Fermi level shifted below its intrinsic position except for the C4 configuration, where the ICl molecules resided far from adjacent dopants and in the horizontal orientation outside the CNT. However, this charge-sharing phenomenon created impurity bands at the edge of the valence band in the system with an increase in electrical conductivity. The electrical conductivity increased in the ICl-doped CNT system due to impurity band formation,

Table 2 The alteration of the band gap and peak values of thermoelectric transport parameters at different doping orientations at 300 temperature

Configuration	Bandgap (eV)	S_{max} (μV K^{-1})	σ_{max} (kS m^{-1})	PF$_{max}$ (mW m^{-1} K^{-2})
C1	0.65	1003	292	2.40
C2	0.66	946	168	0.41
C3	0.55	952	228	0.82
C4	0.48	785	150	0.90
C5	0.55	944	228	1.82
C6	0.57	919	239	2.10

consequently enhancing the power factor. The greater interaction of the host and dopants occurred when the ICl molecules were closely spaced in vertical orientations, especially inside the tube (C1). This was reflected in their thermoelectric power factor, evident from their respective plots. The σ for the C1 configuration elevated to 40 kS m^{-1} and can further be increased to 292 kS m^{-1} by further doping the CNT bundle. In addition to that, the thermoelectric power factor of the ICl-doped SWCNT network enhanced by 0.28 mW m^{-1} K^{-2} for the C1 configuration at their Fermi level and can further be amplified to 2.4 mW m^{-1} K^{-2}, approximately an eight-fold increment by additionally doping the CNT. In summary, charge sharing between the host and dopants increased when the ICl molecules were in close spacing, which contributed to its power factor enhancement. The peak of the thermoelectric power factor appeared at the n-type region when the ICl molecules were inside the tube. However, the peak performance occurred at the p-type region when the ICl molecules were outside the tube. Our findings will be beneficial in designing and fabricating CNT fiber-based wearable electronic and thermoelectronic devices.

Author contributions

Md. Mafizul Islam: conceptualization, formal analysis, methodology, visualization, software, investigation, writing – original draft. Ahmed Zubair: supervision, conceptualization, methodology, visualization, project administration, resources, writing – original draft, writing – review & editing.

Data availability

Data for this article are available at github at **https://github.com/ahmedzubair003/ICldopedCNT.git**.

Conflicts of interest

There are no conflicts to declare.

Acknowledgements

Notes and references

1 N. T. Hung, A. R. T. Nugraha and R. Saito, *Energies*, 2019, **12**, 4561.

2 *CRC Handbook of Thermoelectrics*, ed. D. M. Rowe, CRC Press, Boca Raton, FL, 1995.

3 F. Islam, A. Zubair and N. Fairuz, 2019 IEEE Student Conference on Research and Development (SCOReD), 2019, pp. 253–258.

4 J. Duan, X. Wang, X. Lai, G. Li, K. Watanabe, T. Taniguchi, M. Zebarjadi and E. Y. Andrei, *Proc. Natl. Acad. Sci. U. S. A.*, 2016, **113**, 14272–14276.

5 S. Shimizu, J. Shiogai, N. Takemori, S. Sakai, H. Ikeda, R. Arita, T. Nojima, A. Tsukazaki and Y. Iwasa, *Nat. Commun.*, 2019, **10**, 825.

6 D. M. Rowe and G. Min, *J. Mater. Sci. Lett.*, 1995, **14**, 617–619.

7 L. D. Hicks and M. S. Dresselhaus, *Phys. Rev. B: Condens. Matter Mater. Phys.*, 1993, **47**, 16631–16634.

8 L. D. Hicks and M. S. Dresselhaus, *Phys. Rev. B: Condens. Matter Mater. Phys.*, 1993, **47**, 12727–12731.

9 M. Dresselhaus, G. Chen, M. Tang, R. Yang, H. Lee, D. Wang, Z. Ren, J.-P. Fleurial and P. Gogna, *Adv. Mater.*, 2007, **19**, 1043–1053.

10 A. Zubair, X. Wang, F. Mirri, D. E. Tsentalovich, N. Fujimura, D. Suzuki, K. P. Soundarapandian, Y. Kawano, M. Pasquali and J. Kono, *Phys. Rev. Mater.*, 2018, **2**, 015201.

11 J.-P. Salvetat, J.-M. Bonard, N. Thomson, A. Kulik, L. Forró, W. Benoit and L. Zuppiroli, *Appl. Phys. A: Mater. Sci. Process.*, 1999, **69**, 255–260.

12 N. T. Hung and R. Saito, *Adv. Quantum Technol.*, 2021, **4**, 2000115.

13 G. D. Mahan and J. O. Sofo, *Proc. Natl. Acad. Sci. U. S. A.*, 1996, **93**, 7436–7439.

14 X. Zhang and Y. Pei, *npj Quantum Mater.*, 2017, **2**, 68.

15 D. Tristant, A. Zubair, P. Puech, F. Neumayer, S. Moyano, R. J. Headrick, D. E. Tsentalovich, C. C. Young, I. C. Gerber, M. Pasquali, J. Kono and J. Leotin, *Nanoscale*, 2016, **8**, 19668–19676.

16 A. Zubair, D. Tristant, C. Nie, D. E. Tsentalovich, R. J. Headrick, M. Pasquali, J. Kono, V. Meunier, E. Flahaut, M. Monthioux, I. C. Gerber and P. Puech, *Phys. Rev. Mater.*, 2017, **1**, 064002.

17 B. Kumanek, K. Z. Milowska, Ł. Przypis, G. Stando, K. Matuszek, D. MacFarlane, M. C. Payne and D. Janas, *ACS Appl. Mater. Interfaces*, 2022, **14**, 25861–25877.

18 S. Hong, J. Nam, S. Park, D. Lee, M. Park, D. S. Lee, N. D. Kim, D.-Y. Kim, B.-C. Ku, Y. A. Kim and J. Y. Hwang, *Carbon*, 2021, **184**, 207–213.

19 N. Behabtu, C. C. Young, D. E. Tsentalovich, O. Kleinerman, X. Wang, A. W. K. Ma, E. A. Bengio, R. F. ter Waarbeek, J. J. de Jong, R. E. Hoogerwerf, S. B. Fairchild, J. B. Ferguson, B. Maruyama, J. Kono, Y. Talmon, Y. Cohen, M. J. Otto and M. Pasquali, *Science*, 2013, **339**, 182–186.

20 I. Puchades, C. C. Lawlor, C. M. Schauerman, A. R. Bucossi, J. E. Rossi, N. D. Cox and B. J. Landi, *J. Mater. Chem. C*, 2015, **3**, 10256–10266.

21 B. Kumanek, G. Stando, P. Stando, K. Matuszek, K. Z. Milowska, M. Krzywiecki, M. Gryglas-Borysiewicz, Z. Ogorzałek, M. C. Payne, D. MacFarlane and D. Janas, *Sci. Rep.*, 2021, **11**, 8649.

22 N. Komatsu, Y. Ichinose, O. S. Dewey, L. W. Taylor, M. A. Trafford, Y. Yomogida, G. Wehmeyer, M. Pasquali, K. Yanagi and J. Kono, *Nat. Commun.*, 2021, **12**, 4931.

23 B. Kumanek, Ł. Przypis, P. S. Wróbel, M. Krzywiecki, K. Z. Walczak and D. Janas, *Appl. Nanosci.*, 2020, **10**, 529–539.

24 S.-H. Jhi, S. G. Louie and M. L. Cohen, *Solid State Commun.*, 2002, **123**, 495–499.

25 D. Janas, K. Z. Milowska, P. D. Bristowe and K. K. K. Koziol, *Nanoscale*, 2017, **9**, 3212–3221.

26 D. Janas, A. P. Herman, S. Boncel and K. K. Koziol, *Carbon*, 2014, **73**, 225–233.

27 S. Ghosh, S. R. K. C. S. Yamijala, S. K. Pati and C. Rao, *RSC Adv.*, 2012, **2**, 1181–1188.

28 P. Giannozzi, S. Baroni, N. Bonini, M. Calandra, R. Car, C. Cavazzoni, D. Ceresoli, G. L. Chiarotti, M. Cococcioni, I. Dabo, A. D. Corso, S. de Gironcoli, S. Fabris, G. Fratesi, R. Gebauer, U. Gerstmann, C. Gougoussis, A. Kokalj, M. Lazzeri, L. Martin-Samos, N. Marzari, F. Mauri, R. Mazzarello, S. Paolini, A. Pasquarello, L. Paulatto, C. Sbraccia, S. Scandolo, G. Sclauzero, A. P. Seitsonen, A. Smogunov, P. Umari and R. M. Wentzcovitch, *J. Phys.: Condens. Matter*, 2009, **21**, 395502.

29 G. Henkelman, A. Arnaldsson and H. Jónsson, *Comput. Mater. Sci.*, 2006, **36**, 354–360.

30 G. K. Madsen and D. J. Singh, *Comput. Phys. Commun.*, 2006, **175**, 67–71.

31 M. M. Islam and A. Zubair, 2022 12th International Conference on Electrical and Computer Engineering (ICECE), 2022, pp. 425–428.

32 D. Dass, *Superlattices Microstruct.*, 2018, **120**, 108–126.

33 N. W. Ashcroft and N. D. Mermin, *Solid State Physics*, Cengage Learning, 1976.

34 M. M. Islam and A. Zubair, *Mater. Adv.*, 2023, **4**, 6553–6567.